PAPER • OPEN ACCESS

Topological Devil's staircase in atomic two-leg ladders

New Journal of Physics
The open access journal at the forefront of physics

Deutsche Physikalische Gesellschaft DPG
IOP Institute of Physics

Published in partnership with: Deutsche Physikalische Gesellschaft and the Institute of Physics

OPEN ACCESS

RECEIVED
6 November 2018

REVISED
3 March 2019

ACCEPTED FOR PUBLICATION
8 March 2019

PUBLISHED
25 April 2019

PAPER

Topological Devil's staircase in atomic two-leg ladders

S Barbarino[1,2,10], D Rossini[3], M Rizzi[4,5,6], R Fazio[7,8], G E Santoro[1,8,9] and M Dalmonte[1,7]

[1] Scuola Internazionale Studi Superiori Avanzati (SISSA), Via Bonomea 265, I-34136, Trieste, Italy
[2] Institute of Theoretical Physics, Technische Universität Dresden, D-01062, Dresden, Germany
[3] Dipartimento di Fisica, Università di Pisa and INFN, Largo Pontecorvo 3, I-56127, Pisa, Italy
[4] Institute für Physik, Johannes Gutenberg-Universität, D-55128, Mainz, Germany
[5] Institute of Quantum Control (PGI-8), Forschungszentrum Jülich, D-52425, Jülich, Germany
[6] Institute for Theoretical Physics, University of Cologne, D-50937, Köln, Germany
[7] International Centre for Theoretical Physics (ICTP), PO Box 586, I-34014, Trieste, Italy
[8] NEST, Scuola Normale Superiore & Istituto Nanoscienze-CNR, I-56126, Pisa, Italy
[9] CNR-IOM Democritos National Simulation Center, Via Bonomea 265, I-34136, Trieste, Italy
[10] Author to whom any correspondence should be addressed

E-mail: simone.barbarino@sns.it

Keywords: fractional topological phase, two-leg ladder, strongly correlated, cold-atoms

Abstract

We show that a hierarchy of topological phases in one dimension—a topological Devil's staircase—can emerge at fractional filling fractions in interacting systems, whose single-particle band structure describes a topological or a crystalline topological insulator. Focusing on a specific example in the BDI class, we present a field-theoretical argument based on bosonization that indicates how the system, as a function of the filling fraction, hosts a series of density waves. Subsequently, based on a numerical investigation of the low-lying energy spectrum, Wilczek–Zee phases, and entanglement spectra, we show that they are symmetry protected topological phases. In sharp contrast to the non-interacting limit, these topological density waves do not follow the bulk-edge correspondence, as their edge modes are gapped. We then discuss how these results are immediately applicable to models in the AIII class, and to crystalline topological insulators protected by inversion symmetry. Our findings are immediately relevant to cold atom experiments with alkaline-earth atoms in optical lattices, where the band structure properties we exploit have been recently realized.

1. Introduction

In the last few years, a series of remarkable experiments has demonstrated how cold atomic gases in optical lattices can realize topological band structures [1–7] with a high degree of accuracy and tunability [8–12]. In the context of one-dimensional (1D) systems, ladders pierced by synthetic gauge fields [13–23] have been experimentally shown to display a plethora of phenomena, including chiral currents [24] and edge modes akin to the two-dimensional Hall effect [7], accompanied with the long-predicted—but hard to directly observe—skipping orbits [25, 26]. While such phenomena have required relatively simple microscopic Hamiltonians apt to describe electrons in a magnetic field [27], the flexibility demonstrated in very recent settings utilizing alkaline-earth-like atoms [28–33] has shown how a new class of model Hamiltonians—where nearest neighbor couplings on multi-leg ladders can be engineered almost independently one from the other—is well within experimental reach. Remarkably, these works have not only demonstrated the capability of realizing spin–orbit couplings utilizing clock transitions [29, 30], but also the observation of band structures where topology is tied to inversion symmetry [31, 34], a playground for crystalline topological insulators [35–37]. A natural question along these lines is whether these new recently developed setups offer novel opportunities for the observation of intrinsically interacting topological phases—e.g. symmetry-protected topological phases which appear at fractional filling fractions.

In this work, we show how, starting from experimentally realized microscopic Hamiltonians [31], interactions can generically stabilize novel topological phases in regimes where single-particle Hamiltonians

cannot host any. We consider a 1D ladder with two internal spin states, supporting a topological phase at integer filling, and we show that, when the particle filling is reduced to a fractional value, repulsive interactions can stabilize a hierarchy of unconventional topological gapped phases, namely a topological Devil's staircase [38, 39]. Such topological density-wave phases are characterized by a well-defined topological number, the Wilczek–Zee phase [40, 43], thus signaling that the topological properties of the non-interacting bands are inherited at fractional fillings in the presence of interactions. These gapped states present a degenerate entanglement spectrum [44–46] and, in some regimes, an unconventional edge physics without zero-energy modes.

The appearance of these fractional topological phases is reminiscent of the quantum Hall physics, where a similar transition from the integer to the fractional regime is observed when interactions are considered. Owing to the 1D context, here the main difference is that all the phases are symmetry-protected topological phases, as true topological order cannot take place. We note that, for specific filling fractions, our results are closely related to other topological density waves found in single-band models [47, 48]. The mere existence of a full class of topological density waves is surprising in view of the fact that, typically, non-interacting topological phases at integer filling appearing in the context of 1D systems with two internal spin states such as the Su–Schrieffer–Hegger model [49] or Creutz ladders [50] are robust against weak interactions only, and disappear [51, 52] in the strongly interacting regime[11].

We illustrated the appearance of such phases by studying a model Hamiltonian description for the BDI [49–51] and AIII symmetry classes [52, 54] of the Altland–Zirnbauer classification (AZc) [1, 6], and a crystalline topological insulator case of a 1D model supporting a spatial inversion symmetry protected topological phase at filling one [35–37]. Our results are general in the sense that these fractional phases can be potentially observed in all symmetry classes of the AZc which can be realized in a two-leg ladder. Our work is complementary to recent approaches investigating interaction induced fractional topological insulators [55–63], which typically focus on specific case scenarios that accurately mimic the edge physics of quantum Hall states or extend topological superconductivity at finite interaction strength.

From an experimental perspective, the models we investigate are immediately relevant to cold gases experiments. In particular, recent implementations using alkaline-earth-like atoms such as Yb [25, 29, 32] and Sr [30] have demonstrated an ample degree of flexibility in tuning parameters (including static gauge fields) in two-leg ladders, exploiting the concept of synthetic dimension [64, 65]. Most importantly, the single particle Hamiltonian we discuss below has been realized in a ^{173}Yb gas, see [32], and similar schemes shall be applicable to ^{87}Sr gases as well.

This paper is organized as follows. In section 2 we present the model and discuss its fundamental symmetries. sections 3 and 3.3 contain our main results. In particular, in section 3, we consider models belonging to the BDI and AIII symmetry classes and we show the appearance of a topological fractional phase at filling $\nu = 1/2$ which can be viewed as a precursor of the topological Devil's staircase. We discuss the topological properties of this phase: the Wilczek–Zee phase, and the entanglement spectrum in the ground-state manifold, using numerical methods as Lanczos-based exact diagonalization [66] and density-matrix renormalization group (DMRG) [67, 68] simulations. Finally, we discuss how this topological phase supports edge modes, which, while not at zero energy, can still be diagnosed by simple correlation functions. Then, in section 3.3, by means of a bosonization approach we discuss the appearance of the topological Devil's staircase at lower fillings and we explicitly address the filling $\nu = 1/3$ case. Finally, in section 4 we generalize our results to the case of a crystalline topological insulator. Our conclusions are drawn in section 5.

2. Model and symmetries

Let us start by introducing the Hamiltonian we are going to focus on. For the sake of clarity, we also review the main definitions of time-reversal, particle-hole, and chiral symmetry in the language of second quantization, which is best suited to the case of interacting systems.

2.1. Model Hamiltonian

We consider a 1D chain with L sites along the physical dimension. These are populated by fermionic particles described by the canonical operators $\hat{c}^{(\dagger)}_{j,\sigma}$, annihilating (creating) a fermion at site $j = 1, \ldots, L$, with two internal degrees of freedom labeled by $\sigma = \uparrow, \downarrow$ (resp. $+1, -1$).

[11] This last fact is instead not surprising, once one realizes that, in the presence of a strongly repulsive Hubbard interaction term, such kind of models with nearest-neighbor hopping terms can be mapped onto topologically trivial spin-1/2 XYZ models [53].

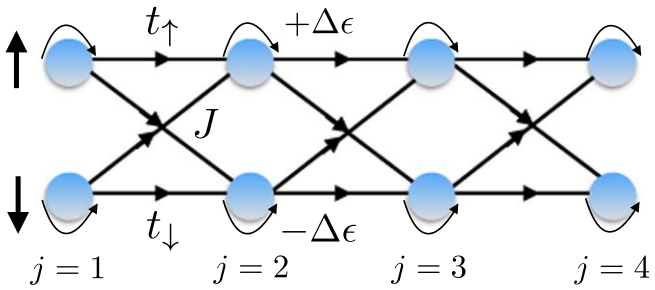

Figure 1. Schematic representation of a 1D chain with two internal spin states, ↑ and ↓. Curved arrows at the dots represent the species-dependent chemical potential $\Delta\epsilon$ which induces an imbalance between spin up and spin down particles. As discussed in table 1, by properly tuning the parameters t_σ and J in equation (3), it is possible to realize non-interacting topological phases belonging to the symmetry classes BDI and AIII of the AZc and an inversion symmetry protected topological phase supporting a non-trivial phase at integer filling (crystalline topological insulator).

Table 1. By properly tuning the parameters t_σ and J in equation (3), it is possible to realize non-interacting topological phases belonging to the symmetry classes BDI and AIII of the AZc and an inversion symmetry protected topological phase supporting a non-trivial phase at integer filling (crystalline topological insulator). A topological phase belonging to the BDI symmetry class is endowed with a time-reversal T, a particle-hole C, and a chiral S symmetry; a topological phase in the AIII symmetry class is endowed with a chiral symmetry only; see also equations (6)–(8).

	$t_\uparrow$	$t_\downarrow$	J	T	C	S
BDI	$+t$	$-t$	$+iJ$	σ_z	σ_x	σ_y
AIII	$+it$	$-it$	$-J$	/	/	σ_y
inv	$+t+\delta$	$-t+\delta$	$+iJ$	/	/	/

The single-particle physics discussed in this work is fully captured by the Hamiltonian (see figure 1)

$$\hat{H}_0 = \hat{H}_{nn} + \hat{H}_{\Delta\epsilon}, \tag{1}$$

where

$$\hat{H}_{\Delta\epsilon} = \Delta\epsilon \sum_{\sigma,j} \sigma\ \hat{c}^\dagger_{j,\sigma}\hat{c}_{j,\sigma} \tag{2}$$

is a species-dependent chemical potential which induces an imbalance between spin up and spin down particles. The Hamiltonian term

$$\hat{H}_{nn} = \sum_{\sigma,j} (t_\sigma\ \hat{c}^\dagger_{j+1,\sigma}\hat{c}_{j,\sigma} + J\ \hat{c}^\dagger_{j+1,\sigma}\hat{c}_{j,-\sigma}) + \text{h.c.} \tag{3}$$

describes spin-preserving and spin-flipping nearest-neighbor hoppings; the parameters t_σ and J can be tuned according to the prescriptions of table 1.

Crucial for the following discussion is the presence of repulsive density–density interaction terms

$$\hat{H}_{\text{int}} = U\sum_j \hat{n}_{j,\uparrow}\hat{n}_{j,\downarrow} + \sum_p V_p \sum_j \hat{n}_j\hat{n}_{j+p}, \tag{4}$$

where $U > 0$ and $V_p > 0$ with $p = 1, 2, ...$; $\hat{n}_{j,\sigma} = \hat{c}^\dagger_{j,\sigma}\hat{c}_{j,\sigma}$ is the density operator and $\hat{n}_j = \sum_\sigma \hat{n}_{j,\sigma}$. The full Hamiltonian is thus defined by

$$\hat{H} = \hat{H}_0 + \hat{H}_{\text{int}} = \hat{H}_{nn} + \hat{H}_{\Delta\epsilon} + \hat{H}_{\text{int}}. \tag{5}$$

The model we discuss has already been experimentally realized in [32]. We refer to this work for specific details on the experimentally achievable parameter regimes.

Hereafter we will set $\hbar = 1$ and express all energy scales in units of the hopping term t. In order to understand the symmetry class to which $\hat{H}$ belongs, it is first convenient to recall the three symmetries classifying the ten classes of the AZc. Then, we also discuss the inversion symmetry operator.

2.2. Fundamental symmetries

The symmetries playing a crucial role in the AZc are the time-reversal $\hat{\mathcal{T}}$, the particle-hole $\hat{\mathcal{C}}$, and the chiral $\hat{\mathcal{S}}$ symmetry. Their action on the fermionic operators $\hat{c}_{j,\sigma}$ reads [6]:

$$\hat{\mathcal{T}}\,\hat{c}_{j,\sigma}\,\hat{\mathcal{T}}^{-1} = T^{*}_{\sigma',\sigma}\hat{c}_{j,\sigma'} \quad \hat{\mathcal{T}}\,\hat{c}^{\dagger}_{j,\sigma}\,\hat{\mathcal{T}}^{-1} = \hat{c}^{\dagger}_{j,\sigma'}T_{\sigma',\sigma} \tag{6}$$

$$\hat{\mathcal{C}}\hat{c}_{j,\sigma}\hat{\mathcal{C}}^{-1} = C_{\sigma',\sigma}\hat{c}^{\dagger}_{j,\sigma'} \quad \hat{\mathcal{C}}\hat{c}^{\dagger}_{j,\sigma}\hat{\mathcal{C}}^{-1} = \hat{c}_{j,\sigma'}C^{*}_{\sigma',\sigma} \tag{7}$$

$$\hat{\mathcal{S}}\,\hat{c}_{j,\sigma}\,\hat{\mathcal{S}}^{-1} = S_{\sigma',\sigma}\hat{c}^{\dagger}_{j,\sigma'} \quad \hat{\mathcal{S}}\hat{c}^{\dagger}_{j,\sigma}\hat{\mathcal{S}}^{-1} = \hat{c}_{j,\sigma'}S^{*}_{\sigma',\sigma}, \tag{8}$$

where T, C, and S are 2×2 unitary matrices satisfying $TT^{*} = CC^{*} = \pm\sigma_0$ (σ_0 being the 2×2 identity matrix) and $S = TC^{*}$, up to an arbitrary phase factor such that $S^2 = \sigma_0$. Furthermore, $\hat{\mathcal{T}}$ and $\hat{\mathcal{S}}$ are anti-unitary (i.e. $\hat{\mathcal{T}}(+i)\hat{\mathcal{T}}^{-1} = \hat{\mathcal{S}}(+i)\hat{\mathcal{S}}^{-1} = -i$), while $\hat{\mathcal{C}}$ is unitary (i.e. $\hat{\mathcal{C}}(+i)\hat{\mathcal{C}}^{-1} = +i$). We also introduce the unitary inversion symmetry operator $\hat{\mathcal{I}}$, which acts as [36]:

$$\hat{\mathcal{I}}\,\hat{c}_{j,\sigma}\,\hat{\mathcal{I}}^{-1} = I_{\sigma',\sigma}\hat{c}_{-j,\sigma'} \quad \hat{\mathcal{I}}\,\hat{c}^{\dagger}_{j,\sigma}\,\hat{\mathcal{I}}^{-1} = \hat{c}^{\dagger}_{-j,\sigma'}I^{*}_{\sigma',\sigma}, \tag{9}$$

where I is again a unitary 2×2 matrix. The Hamiltonian $\hat{H}$ in equation (5) is invariant under a symmetry $\hat{\mathcal{M}}$, with $\hat{\mathcal{M}} = \hat{\mathcal{T}},\ \hat{\mathcal{C}},\ \hat{\mathcal{S}}$, if and only if

$$\hat{\mathcal{M}}\,\hat{H}\,\hat{\mathcal{M}}^{-1} = \hat{H}. \tag{10}$$

Switching off the interaction term, the single-particle Hamiltonian (1) can be conveniently rewritten as:

$$\hat{H}_0 = \sum_k \hat{C}^{\dagger}_k\, H_0(k)\, \hat{C}_k, \tag{11}$$

with $\hat{C}^{\dagger}_k = (\hat{c}^{\dagger}_{k,\uparrow}\ \hat{c}^{\dagger}_{k,\downarrow})$ by means of the momentum-space operators

$$\hat{c}_{k,\sigma} = \frac{1}{\sqrt{L}}\sum_j \mathrm{e}^{-\mathrm{i}kj}\hat{c}_{j,\sigma}, \quad \text{with} \quad k \in [-\pi,\,\pi). \tag{12}$$

Then the requirements (6)–(9) lead to the more familiar ones [6]:

$$\hat{\mathcal{T}}\,\hat{H}_0\,\hat{\mathcal{T}}^{-1} = \hat{H}_0 \rightarrow T\,H^{*}_0(k)\,T^{\dagger} = H_0(-k) \tag{13}$$

$$\hat{\mathcal{C}}\,\hat{H}_0\,\hat{\mathcal{C}}^{-1} = \hat{H}_0 \rightarrow C\,H^{*}_0(k)\,C^{\dagger} = -H_0(-k) \tag{14}$$

$$\hat{\mathcal{S}}\,\hat{H}_0\,\hat{\mathcal{S}}^{-1} = \hat{H}_0 \rightarrow S\,H_0(k)\,S^{\dagger} = -H_0(k) \tag{15}$$

$$\hat{\mathcal{I}}\,\hat{H}_0\,\hat{\mathcal{I}}^{-1} = \hat{H}_0 \rightarrow I\,H_0(k)\,I^{\dagger} = H_0(-k). \tag{16}$$

According to the AZc, in 1D only five symmetry classes (BDI, AIII, D, CII, and DIII) can support a topological phase (assuming no spatial symmetry). In the next section we will consider interacting topological models whose single-particle Hamiltonians belong to the symmetry classes BDI [51] and AIII [52, 54] and which can be realized in two-leg ladders with nearest-neighbor couplings, by properly tuning the coefficients t_σ and J in the Hamiltonian term $\hat{H}_{nn}$ of equation (3), according to the prescriptions of table 1. On the other hand, CII and DIII models require ladders with a higher number of legs, or two-leg ladders in the presence of next-nearest-neighbor hopping terms, and will not be considered here.

At integer filling, $\nu = N/L = 1$ (where N is the number of fermions), models in [51, 52, 54] can exhibit a topological phase characterized by the presence of exponentially localized zero-energy edge modes in the non-interacting spectrum, a quantized Zak phase, and a doubly degenerate entanglement spectrum [44, 45]. Conversely, in the present context we are interested in investigating the topological properties when the particle filling is fractional, i.e. $\nu = 1/q$, with $q > 1$ integer. We will also consider ladders supporting a crystalline topological phase protected by the spatial inversion symmetry, which cannot be understood in terms of the standard AZc (section 4).

3. Topological phases emerging due to interactions at fractional fillings in BDI and AIII band structures

Firstly we focus on two-leg ladder whose non-interacting Hamiltonian is in the BDI symmetry class. In this case, the various parameters are fixed (see table 1), and the resulting Hamiltonian of equation (5) reads:

$$\hat{H} = \sum_{\sigma,j}(\sigma t\ \hat{c}^{\dagger}_{j+1,\sigma}\hat{c}_{j,\sigma} + iJ\ \hat{c}^{\dagger}_{j+1,\sigma}\hat{c}_{j,-\sigma} + \text{h.c.}) + \Delta\epsilon\sum_{\sigma,j}\sigma\ \hat{c}^{\dagger}_{j,\sigma}\hat{c}_{j,\sigma} + \hat{H}_{\text{int}}. \tag{17}$$

Using equations (6)–(8), and the matrices defined in table 1, it is easy to observe that $\hat{\mathcal{T}}\,\hat{H}\,\hat{\mathcal{T}}^{-1} = \hat{H}$, while $\hat{\mathcal{C}}\,\hat{H}\,\hat{\mathcal{C}}^{-1} = \hat{H}$ and $\hat{\mathcal{S}}\,\hat{H}\,\hat{\mathcal{S}}^{-1} = \hat{H}$ up to constant terms, $UL + 4\sum_p V_p$, and trivial chemical potential terms

$(-U - 2\sum_p V_p)\sum_j \hat{n}_j$. In the following we will focus on fractional fillings $\nu = 1/q$, and consider repulsive interactions. Our results for the BDI symmetry class are immediately applicable to the model in the AIII class, which can be obtained from to latter via the unitary transformation also known as Kawamoto–Smit rotation in the context of Lattice Field Theories [74] $\hat{\mathcal{U}}_j \hat{c}_{j,\sigma}\, \hat{\mathcal{U}}_j^{-1} = \mathrm{e}^{\mathrm{i}\frac{\pi}{2}j}\hat{c}_{j,\sigma}$ (see again table 1).

3.1. Effective lowest-band Hamiltonian

The single-particle contributions of the Hamiltonian (17), assuming periodic boundary conditions (PBC), can be diagonalized as

$$\hat{H}_0 = \sum_k \sum_\eta \eta\, E(k) \hat{d}^\dagger_{k,\eta}\, \hat{d}_{k,\eta}, \tag{18}$$

with $\eta = \pm 1$, $k \in [-\pi, \pi)$ and

$$E(k) = \sqrt{(2t\cos k + \Delta\epsilon)^2 + 4J^2 \sin^2 k} \tag{19}$$

by means of the unitary transformation $R_k = \exp[\mathrm{i}\theta_k \sigma_y/2]$ such that $R_k^\dagger H_0(k) R_k = E(k)\sigma_z$ with

$$\sin\theta_k = 2J\frac{\sin k}{E(k)}, \quad \cos\theta_k = \frac{2t\cos k + \Delta\epsilon}{E(k)}; \tag{20}$$

we stress here that R_k is defined up to an arbitrary complex phase $\mathrm{e}^{\mathrm{i}\varphi_k}$. Consequently, the operators $\hat{d}_{k,+1}$ and $\hat{d}_{k,-1}$ can be related to the original ones as

$$\begin{cases} \hat{d}_{k,-1} = \mathrm{e}^{\mathrm{i}\varphi_k}\left(\cos\frac{\theta_k}{2}\hat{c}_{k,\uparrow} + \sin\frac{\theta_k}{2}\hat{c}_{k,\downarrow}\right) \\ \hat{d}_{k,+1} = \mathrm{e}^{\mathrm{i}\varphi_k}\left(-\sin\frac{\theta_k}{2}\hat{c}_{k,\uparrow} + \cos\frac{\theta_k}{2}\hat{c}_{k,\downarrow}\right). \end{cases} \tag{21}$$

In order to probe the existence of a hierarchy of fully gapped phases at fractional fillings, we conveniently introduce the real-space fermionic operators $\hat{d}_{j,\eta} = \sqrt{L}^{-1}\sum_k \mathrm{e}^{\mathrm{i}kj}\hat{d}_{k,\eta}$ built up from the momentum-space operators $\hat{d}_{k,\eta}$ defined in equation (21). Then we remap the original fermionic operators $\hat{c}_{j,\sigma}$ onto the new ones $\hat{d}_{j,\eta}$ as

$$\begin{cases} \hat{c}_{j,\uparrow} = \sum_\ell [F_c(j-\ell)\hat{d}_{\ell,-1} - F_s(j-\ell)\hat{d}_{\ell,+1}] \\ \hat{c}_{j,\downarrow} = \sum_\ell [F_s(j-\ell)\hat{d}_{\ell,-1} + F_c(j-\ell)\hat{d}_{\ell,+1}] \end{cases}, \tag{22}$$

where

$$\begin{cases} F_s(j-\ell) = \frac{1}{L}\sum_k \mathrm{e}^{\mathrm{i}k(j-\ell)}\mathrm{e}^{-\mathrm{i}\varphi_k}\sin\frac{\theta_k}{2} \\ F_c(j-\ell) = \frac{1}{L}\sum_k \mathrm{e}^{\mathrm{i}k(j-\ell)}\mathrm{e}^{-\mathrm{i}\varphi_k}\cos\frac{\theta_k}{2} \end{cases} \tag{23}$$

are the Wannier functions of the tight-binding model; in the following, we assume $\varphi_k = 0$. For this choice of φ_k, the Wannier functions $F_c(j-\ell)$ and $F_s(j-\ell)$ can be calculated exactly when $\Delta\epsilon = 0$, as shown in appendix A. When $\Delta\epsilon > 0$, the functions $F_c(j-\ell)$ and $F_s(j-\ell)$ can be calculated numerically. However, we have verified that the functions $F_c(j-\ell)$ and $F_s(j-\ell)$ exhibit a weak dependence on $\Delta\epsilon$ and their expressions calculated for $\Delta\epsilon = 0$ are a good approximation as long as $\Delta\epsilon \langle\langle t$.

To simplify the problem, we project on the lowest band by assuming that the interaction terms U and V_p are much smaller than the band gap, i.e. $\approx 4J$ when $J = t$ and $\Delta\epsilon = 0$. Since we are dealing with low fillings anyway, it is reasonable to suppose that only the lower band is significantly populated (from now on, we will thus omit the index -1). In order to check the self-consistency of our predictions, numerical simulations will nonetheless be performed with the full description of the system. Under these assumptions, $\hat{H}_0$ becomes

$$\hat{H}_0 = \sum_{j,\ell} [\mathcal{E}(\ell - j)\, \hat{d}^\dagger_j \hat{d}_\ell + \text{h.c.}] \tag{24}$$

with $\mathcal{E}(\ell - j) = \frac{1}{L}\sum_k E(k)\, \mathrm{e}^{\mathrm{i}k(\ell-j)}$. Of course, the Hamiltonian (24) is highly non-local, since all sites are coupled together by long-range terms However, as shown in figure 2, the coefficient $\mathcal{E}(\ell - j)$ decays exponentially with $\ell - j$ and the lower band can be approximated by truncating to nearest-neighbor terms:

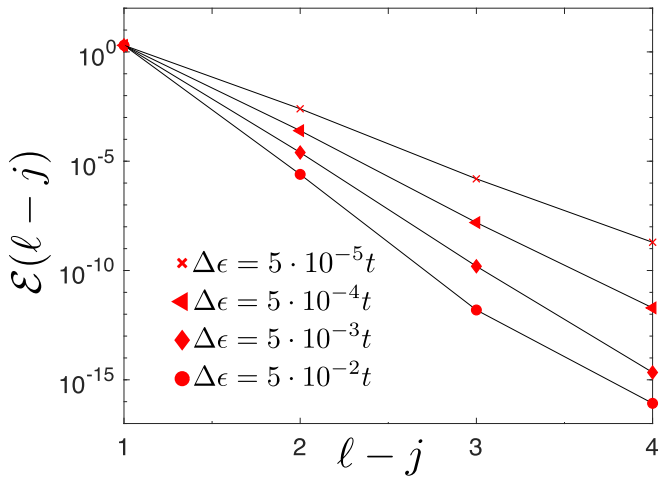

Figure 2. The effective coupling $\mathcal{E}(\ell - j)$ with $J = t$ for different values of $\Delta\epsilon$; for $j = \ell$ we get a constant contribution which can be neglected.

$$\hat{H}_0 \approx -\mathcal{E}_1 \sum_j (\hat{d}^\dagger_{j+1}\hat{d}_j + \text{h.c.}), \tag{25}$$

where we have defined $\mathcal{E}_1 \equiv -\mathcal{E}(1)$ and neglected an inessential chemical potential. For $J = t$, it turns out that $\mathcal{E}_1 = \Delta\epsilon/2$. We stress here that, a truncation up to nearest-neighbor terms only breaks the symmetries of the original model and the new Hamiltonian $\hat{H}_0$ is not topological. Nevertheless this approach is useful to show the appearance of a hierarchy of fully gapped phases. Their topological properties will be discussed in the following (see below).

Let us focus on the interaction terms By means of the mapping (22) and considering the dominant contributions, it is possible to approximate $\hat{c}_{j,\uparrow} \approx F_c(1)\hat{d}_{j+1} + F_c^*(1)\hat{d}_{j-1}$ and $\hat{c}_{j,\downarrow} \approx F_s(0)\hat{d}_j$. Then, the Hubbard interaction term $U\hat{n}_{j,\uparrow}\hat{n}_{j,\downarrow}$ is mapped onto a nearest-neighbor density–density interaction term of the form $\hat{n}_j\hat{n}_{j+1}$ with $\hat{n}_j = \hat{d}^\dagger_j\hat{d}_j$, plus additional contributions (see below). Similarly, the density–density terms $V_p\hat{n}_j\hat{n}_{j+p}$ in the original model will be mapped onto density–density terms of the form $\hat{n}_j\hat{n}_{j+p+1}$. These density–density interaction terms lead to a hierarchy of gapped phases supporting density-wave states at rational filling fractions —the well-known Devil's staircase [38, 39, 69], which we now discuss in the context of our model. In the next paragraph 3.2 we address in detail the filling $\nu = 1/2$, then we generalize our results to lower fillings and we explicitly consider the filling $\nu = 1/3$ in section 3.3.

3.2. Topological density-wave at $\nu = 1/2$: analytical and numerical characterization

In this paragraph we focus on a fractional topological phase at filling $\nu = 1/2$ whose appearance can be discussed in a transparent way, both analytically (by means of a mean-field approach) and numerically (using exact diagonalization and DMRG). Firstly we estimate the critical interaction which stabilizes a gapped phase. To this aim we rewrite the interaction term $\hat{n}_{j,\downarrow}\hat{n}_{j,\uparrow}$ using the mapping (22) approximated at the first non-trivial order, i.e. $\hat{c}_{j,\uparrow} \approx F_c(1)\hat{d}_{j+1} + F_c^*(1)\hat{d}_{j-1}$ and $\hat{c}_{j,\downarrow} \approx F_s(0)\hat{d}_j$ and projecting on the lowest band. Omitting terms which vanish because of the Pauli principle, we obtain

$$\hat{H}_U \approx \tilde{U}\sum_j \left[\hat{n}_j\hat{n}_{j+1} - \frac{1}{2}(\hat{n}_j\hat{d}^\dagger_{j+1}\hat{d}_{j-1} + \text{h.c.})\right], \tag{26}$$

with $\tilde{U} = 2U|F_c(0)|^2|F_s(1)|^2$. Within a mean-field approach, the correlated hopping term $\hat{n}_j\hat{d}^\dagger_{j+1}\hat{d}_{j-1}$ can be neglected (see appendix C for details), and the effective Hamiltonian given by equation (25) plus the density–density interaction term of equation (26) is equivalent to a spin-1/2 XXZ model, which can be exactly solved [71]. The critical interaction U_c stabilizing an antiferromagnetic gapped phase is

$$U_c \sim \frac{\Delta\epsilon}{2|F_c(0)|^2|F_s(1)|^2}, \tag{27}$$

where the functions F_c and F_s were defined in equation (23); in the case of filling $\nu = 1/2$, a gapped phase can be stabilized by the Hubbard interaction only, for this reason, in the following, longer range interaction terms V_p are set to zero.

To substantiate our analytic predictions, assuming PBC conditions, we have numerically computed by means of a Lanczos-based exact diagonalization approach the charge gap of the interacting Hamiltonian (17)

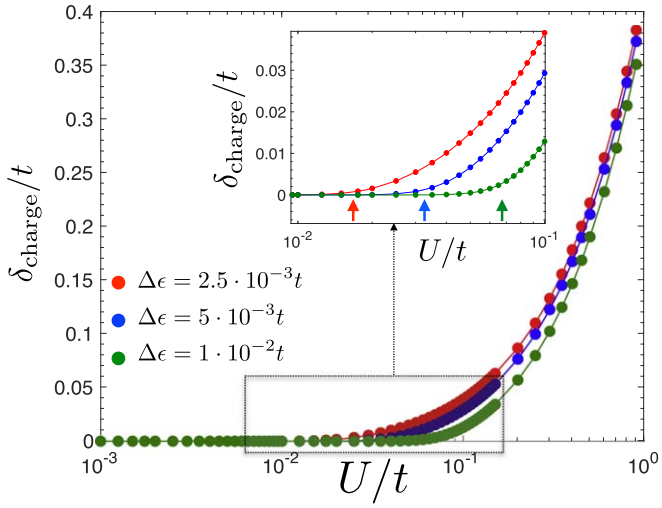

Figure 3. Charge gap $\delta_{\rm charge}$ at filling $\nu = 1/2$ as a function of U/t, for different values of $\Delta\epsilon$, and assuming PBC. The gap $\delta_{\rm charge}$ is obtained by performing a finite-size scaling [75] of numerical exact diagonalization data for $L = 4, \ldots, 14$, with $\delta_{\rm charge}(L) = \delta_{\rm charge} + b/L + c/L^2$. Inset: magnification of the region inside the box; arrows indicate the critical interaction U_c, see equation (27).

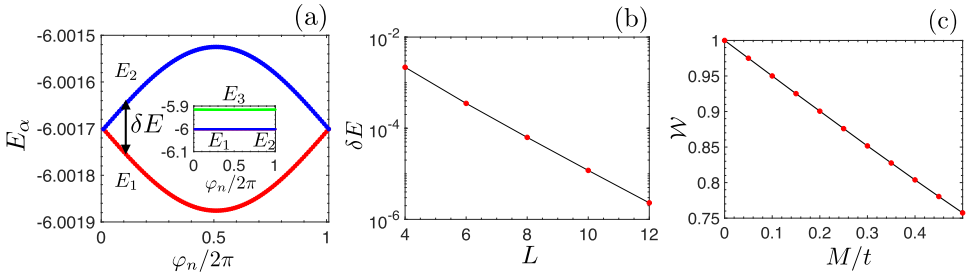

Figure 4. (a) Ground-state energies E_1 and E_2 as a function of the twisting angle φ_n. The inset displays the same plot, for the first three levels, on an enlarged energy scale energies. As expected, the gap between E_1 and E_2 and the first excited state E_3 is preserved when $\varphi_n \neq 0$. (b) The difference $\delta E \equiv E_2 - E_1$ scales exponentially with the chain length L (here $\varphi_n = \pi$). (c) The Wilczek–Zee phase as a function of the symmetry-breaking Hamiltonian term M of equation (34). As expected, for $M = 0$, the Wilczek–Zee phase is quantized to one. Data have been obtained through exact diagonalization, with $U = 0.4t$, $\Delta\epsilon = 10^{-2}t$, and $N_\varphi = 100$. Panel (a) is for $L = 6$, while panels (c)–(d) are for $L = 8$.

$$\delta_{\rm charge} = E_1(N) - \frac{1}{2}[E_1(N+1) + E_1(N-1)], \tag{28}$$

where $E_\alpha(N)$ is the energy of the αth state with N particles (E_1 being the ground-state energy), and here we set $N = L/2$. Figure 3 displays $\delta_{\rm charge}$ as a function of the interaction parameter U/t, for different values of the imbalance term $\Delta\epsilon$. We observe a good agreement of the analytic prediction (27) for the critical interaction U_c, with the point at which the charge gap closes.

Likewise, the charge neutral gap

$$\delta_{{\rm spin},\alpha} = E_\alpha(N) - E_1(N) \tag{29}$$

can be obtained following a similar procedure. In particular, since the ground state always exhibits a two-fold degeneracy (see below), we consider $\alpha = 3$. The behavior of the spin gap $\delta_{\rm spin,3}$ as a function of the interaction parameter U/t is qualitatively analogous to the one of the charge gap (data not shown).

3.2.1. Ground-state degeneracy

Before addressing the topological properties of the fractional phase, it is worth investigating the spectrum $\{E_\alpha(N)\}$ with $\alpha = 1, 2, \ldots$and $N = L/2$, for both PBC and open boundary conditions (OBC). Our numerics evidences how the ground-state degeneracy does indeed depend on the choice of the boundary conditions: while for PBC it is doubly degenerate, see figure 4(a), for OBC it is non-degenerate [45, 72, 73].

To explain the reason of this anomalous degeneracy, we perform the unitary transformation $\hat{\mathcal{U}}_j\, \hat{c}_{j,\sigma}\, \hat{\mathcal{U}}_j^{-1} = e^{i\frac{\pi}{2}j}\hat{c}_{j,\sigma}$ and introduce the 'cage operators'

$$\hat{\gamma}^{\dagger}_{j,\pm} = \frac{1}{2}(\mathrm{i}\hat{c}^{\dagger}_{j,\uparrow} + \hat{c}^{\dagger}_{j,\downarrow}) \mp \frac{1}{2}(\hat{c}^{\dagger}_{j+1,\uparrow} + \mathrm{i}\hat{c}^{\dagger}_{j+1,\downarrow}), \tag{30}$$

which span four lattice sites (of shape 2×2). Then, in the simple case $t = J, \Delta\epsilon = 0$, the Hamiltonian (17) can be rewritten as

$$\hat{H} = -2t\sum_{j}(\hat{\gamma}^{\dagger}_{j,-}\hat{\gamma}_{j,-} - \hat{\gamma}^{\dagger}_{j,+}\hat{\gamma}_{j,+}) + \hat{H}_U. \tag{31}$$

If we now consider the regime where $U \ll t$ and get rid of the upper band, we realize that $\hat{H}_U$ corresponds to a nearest-neighbor interaction term between the cages, i.e. $\hat{n}_{j,-}\hat{n}_{j+1,-}$, with $\hat{n}_{j,-} = \hat{\gamma}^{\dagger}_{j,-}\hat{\gamma}_{j,-}$ (see also [52]). Then, since the ground state at filling $\nu = 1/2$ can be schematically represented via the occupation of local cages, we observe that PBC can effectively fit two of those states (where the cages start at odd or even sites, respectively). Conversely, OBC can only accommodate a single one (where the cages start at odd sites). This interpretation also explains the robustness of the ground-state degeneracy when the boundary conditions are twisted in a closed chain, as the rigid cage structure is not sensitive to such a twist—see next subsection. This behavior is akin to the robustness of ground-state degeneracy in true topologically ordered states (see also [48]).

3.2.2. Wilczek–Zee phase

As discussed in the previous paragraph, when PBC or twisted boundary conditions are assumed the ground state at filling $\nu = 1/2$ is gapped and two-fold degenerate. For this reason the correct topological invariant which has to be used to reveal its topological properties is the Wilczek–Zee phase [40–42]

$$\mathcal{W} = \frac{\mathrm{i}}{\pi}\int_0^{2\pi} \mathrm{d}\varphi\ \mathrm{Tr}[\langle\Psi_\alpha(\varphi)|\partial_\varphi|\Psi_\beta(\varphi)\rangle], \tag{32}$$

where $\{|\Psi_\alpha(\varphi)\rangle\}$ are the different degenerate many-body ground states labeled by the index $\alpha = 1, \ldots, D$, here with $D = 2$, while φ is the twisting angle; α and β are the indices over which the trace is performed. Twisted boundary conditions along the physical dimension can be implemented by taking $t \to t\exp(\mathrm{i}\varphi/L)$ and $J \to J\exp(\mathrm{i}\varphi/L)$. The quantity $\mathcal{W}$ in equation (32) can be numerically computed through the procedure of [43]: one first discretizes the angle $\varphi \in [0, 2\pi]$ in N_φ steps of $\delta\varphi = 2\pi/N_\varphi$, each corresponding to the value φ_n ($n = 0, \ldots, N-1$). Then, after solving the Schrödinger equation $\hat{H}(\varphi_n)|\Psi_{n,\alpha}\rangle = E_\alpha(\varphi_n)|\Psi_{n,\alpha}\rangle$ at the nth step, the obtained many-body ground states $|\Psi_{n,\alpha}\rangle$ can be used to build up the Berry connection

$$A_n = \mathrm{Im}\log\det[D_n^{\alpha,\beta}] \quad \text{with } D_n^{\alpha,\beta} = \langle\Psi_{n,\alpha}|\Psi_{n+1,\beta}\rangle. \tag{33}$$

The WZ phase is defined by $\mathcal{W} = \sum_{n=0}^{N-1} A_n$.

First of all, in figure 4(a) we plot the ground-state energies $E_1(\varphi_n)$ and $E_2(\varphi_n)$ as a function of the discretized twisting angle φ_n and observe that the exact degeneracy at $\varphi_n = 0$ is only apparently removed when $\varphi_n \neq 0$. Indeed, as shown in figure 4(b), the difference $\delta E(\varphi_n = \pi) = E_2(\pi) - \mathrm{E}_1(\pi)$ scales exponentially with the system size L. As expected, the inset of figure 4(a) highlights that the neutral gap (29) does not close when twisted boundary conditions are used, as it is essentially insensitive to boundary conditions. Figure 4(c) demonstrates that, in the presence of a chiral symmetry-breaking Hamiltonian term

$$\hat{H}_{\mathrm{SB}} = \mathrm{i}M\sum_j(\hat{c}^{\dagger}_{j,\uparrow}\hat{c}_{j,\downarrow} - \mathrm{h.c.}), \tag{34}$$

i.e. $\hat{\mathcal{S}}\,\hat{H}_{\mathrm{SB}}\,\hat{\mathcal{S}}^{-1} \neq \hat{H}_{\mathrm{SB}}$, the WZ phase is not quantized anymore, thus signaling that the fractional gapped phase is protected by the same symmetry of the integer case. On the contrary, for $M = 0$, the WZ phase is strictly quantized to one independently of the value of $\Delta\epsilon$ (as long as the interaction term U is sufficiently strong to stabilize a gapped phase).

3.2.3. Entanglement spectrum

To substantiate the topological nature of the gapped phase discussed so far, we have investigated the entanglement spectrum of the Hamiltonian (17) by means of DMRG simulations. Such quantity corresponds to the set of the eigenvalues $\{\lambda_\alpha\}$ of the reduced density matrix $\hat{\rho}_\ell = \mathrm{Tr}_{\bar{\ell}}[|\Psi\rangle\langle\Psi|]$ obtained from the system's ground state $|\Psi\rangle$. Here we consider a subsystem containing $\ell < L$ adjacent sites, and call $\bar{\ell}$ its complement; we note that the degeneracy of the entanglement spectrum is not altered when other values of ℓ are considered. It is well known [44, 45] that there exists a connection between the topological versus trivial nature of $|\Psi\rangle$ and the degeneracy of the eigenvalues of $\hat{\rho}_\ell$. A topological phase corresponds to a degenerate entanglement spectrum: this is indeed what we observe in figure 5, where we plot the first twelve eigenvalues of the entanglement spectrum for a chain of $L = 100$ sites, $U = t$ and $\Delta\epsilon = 2 \times 10^{-2}t$. The upper inset is a magnification of the two largest eigenvalues, whose degeneracy is removed in the presence of the symmetry breaking Hamiltonian term (34)—see the lower inset.

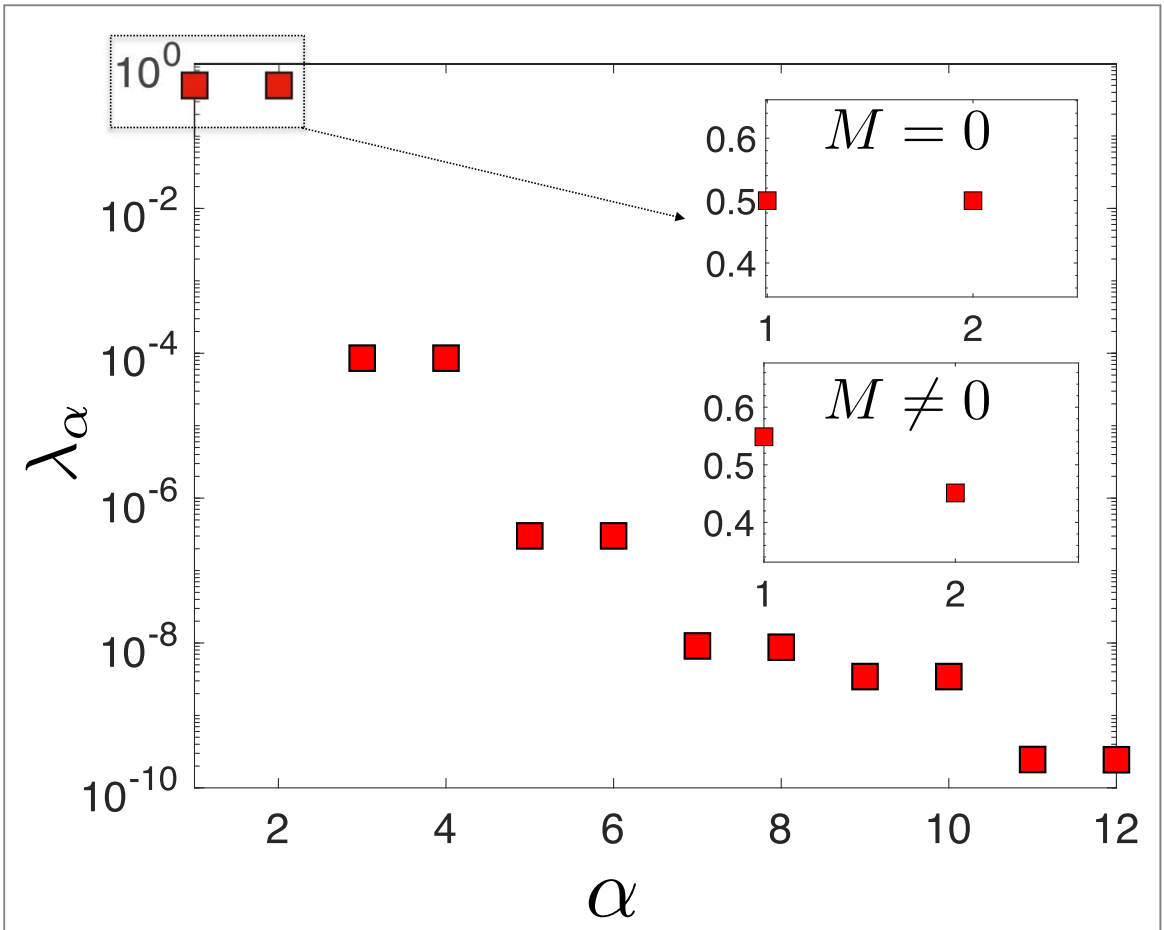

Figure 5. Entanglement spectrum for a chain of $L = 100$ sites, $U = t$ and $\Delta\epsilon = 2 \times 10^{-2}t$; in the present case $\ell = L/2$. Upper inset: magnification of the two largest eigenvalues. Lower inset: the two largest eigenvalues in the presence of the chiral symmetry-breaking term (34), with $M = 0.2t$.

3.2.4. Unconventional edge physics at $\nu = 1/2$

Topological phases are typically characterized by the presence of zero-energy modes, when OBC along the physical dimension are assumed. A necessary but non sufficient condition for their presence is a vanishing (resp. non-vanishing) single-particle charge gap at filling $\nu = 1/2$ with OBC (resp. PBC). Here, despite the topological nature of the model, zero-energy modes do not appear, since the single-particle charge gap remains finite even with OBC, and exhibits a behavior qualitatively analogous to the PBC case—see figure 3.

Although zero-energy modes are absent, the topological nature of the model manifests itself in an unconventional edge physics which can be revealed through the quantity

$$\delta n_j = \langle L/2 + 1|\hat{n}_j|L/2 + 1\rangle - \langle L/2|\hat{n}_j|L/2\rangle, \tag{35}$$

measuring the difference between the expectation value of the density operator onto the state $|L/2\rangle$ corresponding to filling $\nu = 1/2$, and its expectation value onto the state $|L/2 + 1\rangle$ corresponding to filling $\nu = 1/2 + 1/L$.

We start investigating the case where the spin imbalance $\Delta\epsilon$ vanishes. In figure 6 we plot the two density profiles both in the non-interacting case where the phase is gapless, and in the interacting case, for a sufficiently large interaction term U which stabilizes the topological gap. In the non-interacting case (panel (a)), where the quantity δn_j describes the wave-function of the added particle, no edge physics is observed, since δn_j is delocalized over the entire chain. On the contrary, in the interacting case (panel (b)), δn_j displays two sharp peaks close to the edges of the system. When a small imbalance term $\Delta\epsilon$ is considered, the behavior of δn_j changes drastically. As shown in figure 7, we still observe some edge physics, but the quantity δn_j is now spread over a number of sites that increases with growing $\Delta\epsilon$.

We now give an intuitive picture of this spreading effect. To this aim we consider the inset of figure 7(a) where a qualitative picture of the spectrum $\{E_1, E_2, ...\}$ of the interacting Hamiltonian is shown at $\nu = 1/2$ and at $\nu = 1/2 + 1/L$, with $\Delta\epsilon = 0$ and OBC. In the first case $|L/2\rangle$, there is a finite gap between the unique ground state and the first excited state. When the local imbalance term $\Delta\epsilon$ is added, the ground state is unmodified as long as $\Delta\epsilon$ is small with respect to the gap. In the second case $|L/2 + 1\rangle$, the ground state is not protected by a

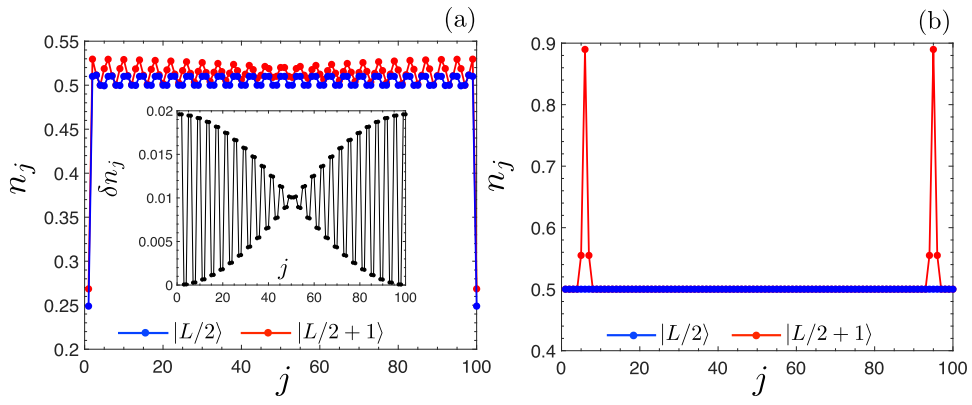

Figure 6. Expectation value of the density operator $\hat{n}_j$ at $\nu = 1/2$ (blue) and $\nu = 1/2 + 1/L$ (red), for $U = 0$ (panel (a), exact diagonalization) and for $U = t$ (panel (b), DMRG). The inset shows the quantity δn_j. Here $J = 0.99t$, $\Delta\epsilon = 0$, and $L = 100$.

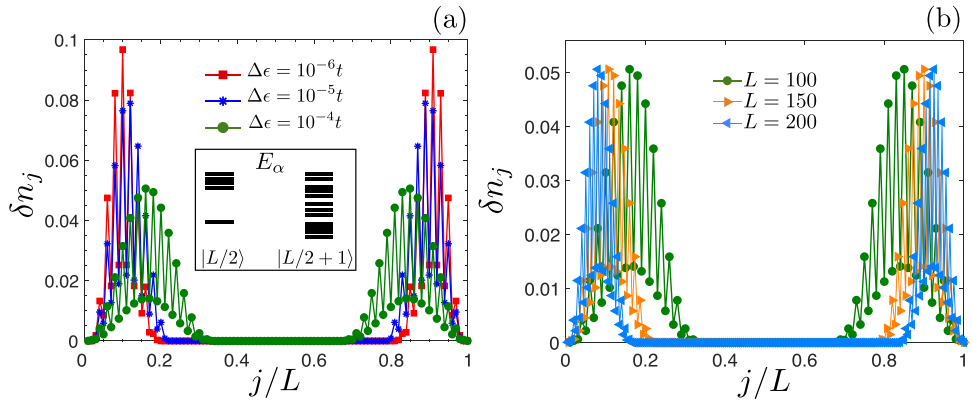

Figure 7. The quantity δn_j for different values of the imbalance $\Delta\epsilon$ and fixed $L = 100$ (panel (a)), and for different sizes L and fixed $\Delta\epsilon = 10^{-4}t$ (panel (b)). Here $J = 0.99t$, $U = t$. Data have been obtained by means of DMRG.

finite energy difference. For this reason, in the presence of the imbalance term $\Delta\epsilon$, it is expected to be a quantum superposition of the ground state $|L/2 + 1\rangle$ at $\Delta\epsilon = 0$ plus pieces coming from the excited states which carry bulk contributions, and originate the spreading of the quantity δn_j shown in figure 7. However, the spreading of δn_j in the bulk becomes negligible in thermodynamic limit, as shown in figure 7(b) for different sizes of the chain.

3.3. Devil's staircase from bosonization

So far we have considered the fractional topological phase at filling $\nu = 1/2$. The appearance of a hierarchy of topological gapped phases at lower fillings can be explained in terms of a bosonization approach [69]. To this aim, we consider the continuum limit of the fermionic operators $\hat{d}_j$, definined by $\hat{d}_j \equiv \hat{d}(x)/\sqrt{a}$ and $\hat{d}_{j+1} \equiv \hat{d}(x + a)/\sqrt{a}$, with a being a generic cut-off length (in the following, $a = 1$). This operator can be expressed in terms of the bosonic fields $\hat{\phi}(x)$ and $\hat{\theta}(x)$ satisfying $[\hat{\phi}(x),\ \partial_{x'}\hat{\theta}(x')] = \mathrm{i}\pi\delta(x - x')$ as

$$\hat{d}(x) = \sum_p A_p\, \mathrm{e}^{-\mathrm{i}(2p+1)[k_F x - \hat{\phi}(x)]}\, \mathrm{e}^{\mathrm{i}\hat{\theta}(x)}, \tag{36}$$

with $k_F = \pi N/L$ being the Fermi momentum. Moreover, the density operator $\hat{\rho}(x) = \hat{d}^\dagger(x)\hat{d}(x)$ is given by

$$\hat{\rho}(x) = -\frac{\partial_x\hat{\phi}(x)}{\pi} + \sum_{p\neq 0} B_p\, \mathrm{e}^{2\mathrm{i}p[k_F x - \hat{\phi}(x)]}; \tag{37}$$

here A_p and B_p are non-universal coefficients which depend on the cut-off length of the theory. Within bosonization, the Hamiltonian (25) plus the density–density interaction terms can be recast into a quadratic form

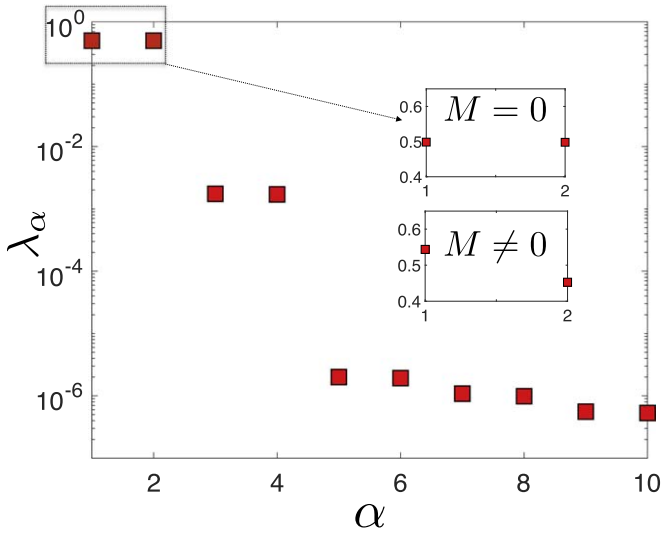

Figure 8. Entanglement spectrum for a chain of $L = 60$ sites, $U = 0$, $V_1 = t$ and $\Delta\epsilon = 8 \times 10^{-2} t$ at filling $\nu = 1/3$. Upper inset: magnification of the two largest eigenvalues. Lower inset: the two largest eigenvalues in the presence of a chiral symmetry-breaking term (34), with $M = 0.2t$.

$$\hat{H}_{\rm bos} = \frac{u}{2\pi} \int {\rm d}x \left[\frac{1}{K} (\partial_x \hat{\phi})^2 + K (\partial_x \hat{\theta})^2 \right] \tag{38}$$

describing a critical gapless theory, plus a sum of sine-Gordon terms

$$\hat{H}_{\rm sg} = \sum_{p>2} M_p \int {\rm d}x \, \cos\left[2p(\hat{\phi}(x) + k_F x)\right], \tag{39}$$

where u is an effective Fermi velocity, K is related to the strength of the interaction terms, while the coefficients M_p represent the amplitudes of the sine-Gordon terms An exact mapping of the quantities u, K, and M_p onto the microscopic parameters is beyond the scope of the present discussion and is generally challenging, due to the complex non-local character of the effective interactions. Furthermore, as shown in appendix B, at filling $\nu = 1/2$, all interaction terms which cannot be recast into a density–density form and which have been so far neglected, lead to a renormalization of the coefficients u, K and M_p only.

Sine-Gordon terms (39) are responsible for the appearance of the gapped phases at fractional fillings. Indeed, when the space dependent $2pk_Fx$ term in the co-sinusoidal functions vanishes, i.e. $2p\, k_F \propto 2\pi$, they become relevant for $K < 2/p^2$ and open a gap. We stress that, within the present bosonization approach, we cannot say anything about the topological properties of these phases. In the case of filling $\nu = N/L = 1/2$, i.e. $k_F = \pi/2$, the most relevant sine-Gordon term is the one with $p = 2$. All other phases at lower filling fractions $\nu = 1/q$, with $q > 2$, can be reached by considering sufficiently long-range density–density interaction terms, as in the conventional Devil's staircase scenario [38, 69, 70]. We now explicitly consider the Hamiltonian (17) and discuss the fractional filling case $\nu = 1/3$ for which the topological phase is stabilized by a nearest-neighbor interaction term in equation (4). In figure 8, we plot the first ten eigenvalues of the entanglement spectrum for a chain of $L = 60$ sites, $U = t$, $V_1 = t$, and $\Delta\epsilon = 8 \times 10^{-2} t$. As expected, the two highest eigenvalues are degenerate due to the topological nature of the ground state. Similarly to the case studied previously, we finally observe that their degeneracy is removed in the presence of the symmetry breaking Hamiltonian term (34), as shown in the lower inset, signaling that the fractional topological phase is protected by the same symmetry that protects the non-interacting topological phase at integer filling.

4. Inversion symmetric topological phases at fractional fillings

It is a natural question to inquire whether the mechanism for the stabilization of interaction-induced topological phases at fractional filling fraction is interwound with spatial symmetries (which play a key role in the establishment of conventional Devil's staircase structures). In this section, we discuss an interacting, crystalline topological insulator, where a fractional topological phase appears when considering interaction effects on the top of partly filled topological bands.

In particular, we consider a two-leg ladder which supports, in the non-interacting regime, a crystalline topological phase at filling $\nu = 1$. Following the prescriptions given in figure 1(b), the resulting Hamiltonian reads [35]:

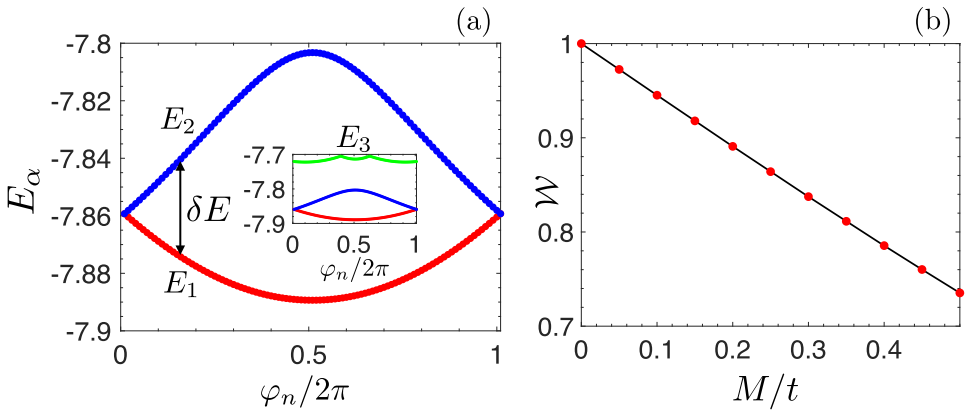

Figure 9. Same plot as in figures 4(a) and (d), but for the Hamiltonian of equation (40) and its symmetry-breaking term M of equation (41). Notice that, analogously to the case studied before, the gap between E_1 and E_2 and the first excited state E_3 is preserved when $\varphi_n \neq 0$. Moreover, under the perturbation M, the WZ phase is not quantized to one anymore. Data have been obtained through exact diagonalization, with $L = 8, \delta = 0.1t, \Delta\epsilon = 10^{-2}t, U = t, N_\varphi = 100$.

$$\hat{H}_0 = \sum_{\sigma,j}[(\sigma t + \delta)\,\hat{c}^\dagger_{j+1,\sigma}\hat{c}_{j,\sigma} + \mathrm{i}J\,\hat{c}^\dagger_{j+1,\sigma}\hat{c}_{j,-\sigma} + \mathrm{h.c.}] + \Delta\epsilon\sum_{\sigma,j}\sigma\,\hat{c}^\dagger_{j,\sigma}\hat{c}_{j,\sigma}, \tag{40}$$

with $\delta \neq 0$. This Hamiltonian, which is not endowed with a particle-hole symmetry nor a chiral symmetry, is characterized by the presence of edge states, by a quantized Zak phase, and by a doubly degenerate entanglement spectrum. Indeed the emerging topologcal phase at filling one is protected by a spatial inversion symmetry [35] $\hat{\mathcal{I}}$ which acts onto the fermionic operators $\hat{c}_{j,\sigma}$ as $\hat{\mathcal{I}}\hat{c}_{j,\sigma}\,\hat{\mathcal{I}}^{-1} = I_{\sigma',\sigma}\hat{c}_{-j,\sigma'}$ such that $\hat{\mathcal{I}}\,\hat{H}\,\hat{\mathcal{I}}^{-1} = \hat{H}$ with $I = \sigma_z$.

In analogy with our previous discussion, we now show that an inversion symmetry protected topological phase at filling $\nu = 1/2$ is stabilized by an on-site repulsive interaction term $\hat{H}_U$ as in equation (4). In order to probe the emerging topological properties, we calculate the ground-state WZ phase (32) following the same procedure discussed for the BDI and AIII symmetry classes.

In figure 9(a) we plot the energies $E_1(\varphi_n)$ and $E_2(\varphi_n)$ of the ground states as a function of the discretized twisting angle φ_n for $\delta = 0.1t$, $\Delta\epsilon = 10^{-2}t$, and $U = t$. The inset shows that the first excited state $E_3(\varphi_n)$ is separated from the ground state by a finite gap. Similarly to the previously studied cases, the exact double degeneracy at $\varphi_n = 0$ of E_1 and E_2 is only apparently removed when $\varphi_n \neq 0$. Indeed, the difference $\delta E(\varphi_n = \pi) = E_2(\pi) - E_1(\pi)$ scales exponentially with the system size (not shown).

Then we introduce an Hamiltonian term

$$\hat{H}_{\mathrm{SB}} = M\sum_j(\hat{c}^\dagger_{j,\uparrow}\hat{c}_{j,\downarrow} + \mathrm{h.c.}), \tag{41}$$

which explicitly breaks the inversion symmetry, i.e. $\hat{\mathcal{S}}\,\hat{H}_{\mathrm{SB}}\,\hat{\mathcal{S}}^{-1} \neq \hat{H}_{\mathrm{SB}}$, and consequently the WZ phase is not quantized anymore.

In figure 9(b) we plot the WZ phase as a function of the inversion symmetry breaking term M. As expected, for $M = 0$ it is quantized and equal to one, while for $M \neq 0$ it is not quantized. This signals that the fractional gapped phase is protected by same symmetry of the integer case, in complete analogy with what observed for the BDI/AIII cases.

5. Conclusions

We have considered a 1D ladder with two internal spin states supporting a topological phase at integer filling and we have shown that, when the particle filling is reduced to a fractional value, repulsive interactions can stabilize a hierarchy of fully gapped density-wave phases with topological features.

In particular we have focused on a specific example in the BDI class (unitarily equivalent to a model in the AIII symmetry class) of the AZc and on a crystalline topological insulator, i.e. a topological model protected by the spatial inversion symmetry. By means of a bosonization approach we have discussed the appearance of a gapped phase at filllings $\nu = 1/q$ and, using exact numerical methods (DMRG simulations and exact diagonalization), we have verified our analytical predictions and we have also characterized the topological properties of the gapped phases at fillings $\nu = 1/2$ and $\nu = 1/3$ by studying the topological quantum number (Wilczek–Zee phase) and the degeneracy of the entanglement spectrum. Considering the effects of perturbations, we have discussed how these fractional topological phases are protected by the same symmetry that protects the non-interacting topological phase at integer filling.

Most importantly, we have shown that these topological density waves do not follow the bulk-edge correspondence, in the sense that they exhibit modes at finite energy localized close to the edges of the system. Their presence has been diagnosed by studying the behavior of the density profile, when an extra particle is put in the system with respect to the filling $\nu = 1/2$. Our results are immediately testable in cold atom experiments described by the setup in [31, 32]: while the single particle Hamiltonian has already been realized, a key requirement is to reach density regimes where an incompressible phase is stabilized in the center of the harmonic trap. Given that fractional phases appear already for quarter-filled band, we expect signal-to-noise not to constitute a problem. Since the incompressible phase in this regime has a gap of order U, this requires cooling in the tens of nanokelvin regime, which is within current experimental reach in these systems [25].

We leave as an intriguing perspective the study of the appearance of these fractional topological phases in topological models belonging to the symmetry classes D, CII, and DIII of the AZc.

Acknowledgments

We thank the CINECA award under the ISCRA initiative for the availability of high performance computing resources and support. MD is supported by the ERC under grant number 758329 (AGEnTh). MD thanks ESI for hospitality during the Quantum Paths Programme. We acknowledge enlightening discussions with Jan Budich, Alexander Nersesyan, and Lorenzo Pastori.

Appendix A. Analytical calculation of $F_c(j-\ell)$

In this appendix we calculate analytically the functions

$$\begin{cases} F_c(j-\ell) = \dfrac{1}{L}\displaystyle\sum_k \mathrm{e}^{\mathrm{i}k(j-\ell)}\cos\frac{\theta_k}{2} \\ F_s(j-\ell) = \dfrac{1}{L}\displaystyle\sum_k \mathrm{e}^{\mathrm{i}k(j-\ell)}\sin\frac{\theta_k}{2} \end{cases} \tag{A.1}$$

for $J = t$ and $\Delta\epsilon = 0$. In this special case, $\cos\theta_k/2 = \cos k/2$. Then, taking into account that

$$\sum_k \mathrm{e}^{\mathrm{i}kj} = \sum_{n=0}^{L-1} \mathrm{e}^{\frac{2\pi\mathrm{i}j}{L}n} \equiv \sum_{n=0}^{L-1} x^n = \begin{cases} L & \text{if } x = 1 \\ \dfrac{1-x^L}{1-x} & \text{if } x \neq 1 \end{cases} \tag{A.2}$$

with $x = \mathrm{e}^{\frac{2\pi\mathrm{i}j}{L}}$, we obtain

$$\begin{cases} F_s(j-\ell) = \dfrac{2}{L}\dfrac{\mathrm{e}^{\frac{2\pi\mathrm{i}(j-\ell)}{L}}\sin\pi/L}{1+\mathrm{e}^{\frac{4\pi\mathrm{i}(j-\ell)}{L}} - 2\mathrm{e}^{\frac{2\pi\mathrm{i}(j-\ell)}{L}}\cos\frac{\pi}{L}} \\ F_c(j-\ell) = \dfrac{2}{L}\dfrac{1-\mathrm{e}^{\frac{2\pi\mathrm{i}(j-\ell)}{L}}\cos\pi/L}{1+\mathrm{e}^{\frac{4\pi\mathrm{i}(j-\ell)}{L}} - 2\mathrm{e}^{\frac{2\pi\mathrm{i}(j-\ell)}{L}}\cos\frac{\pi}{L}}. \end{cases} \tag{A.3}$$

Appendix B. Bosonization at filling $\nu = 1/2$

We discuss how the effective Hamiltonian

$$\hat{H} \approx \hat{H}_0 + \hat{H}_U = -\frac{\Delta\epsilon}{2}\sum_j (\hat{d}^\dagger_{j+1}\hat{d}_{j,} + \text{h.c.}) + \tilde{U}\sum_j \left[\hat{n}_j\hat{n}_{j+1} - \frac{1}{2}(\hat{n}_j\hat{d}^\dagger_{j+1}\hat{d}_{j-1} + \text{h.c.})\right], \tag{B.1}$$

can be attacked by means of a bosonization approach. We introduce the continuum limit operators $\hat{d}(x)$ and $\hat{d}^\dagger(x)$ such that $\hat{d}_j \equiv \hat{d}(x)/\sqrt{a}$ and $\hat{d}_{j+1} \equiv \hat{d}(x+a)/\sqrt{a}$, then the Hamiltonian $\hat{H}_0$ becomes

$$\hat{H}_0 = -\frac{\Delta\epsilon}{2}\int \mathrm{d}x[\hat{d}^\dagger(x+a)\hat{d}(x) + \text{h.c.}]; \tag{B.2}$$

while the interaction term $\hat{H}_U \equiv \hat{H}_U^{(1)} + \hat{H}_U^{(2)}$ becomes

$$\hat{H}_U^{(1)} = \tilde{U}a\int \mathrm{d}x\ \hat{n}(x)\hat{n}(x+a) \tag{B.3}$$

$$\hat{H}_U^{(2)} = -\frac{1}{2}\tilde{U}a\int \mathrm{d}x[\hat{n}(x)\hat{d}^\dagger(x+a)\hat{d}(x-a) + \mathrm{h.c.}] \tag{B.4}$$

here $\tilde{U} = 2UF_c^2(0)|F_s(1)|^2$, while a is the cut-off length of the theory.

To pursue a bosonization approach we introduce the linearized (around the Fermi momentum k_F) fermionic operators $\hat{d}_R(x)$ and $\hat{d}_L(x)$ such that the original fermionic operator $\hat{d}(x)$ can be expanded as $\hat{d}(x) \approx \mathrm{e}^{\mathrm{i}k_F x}\hat{d}_R(x) + \mathrm{e}^{-\mathrm{i}k_F x}\hat{d}_L(x)$ and rewritten as $\hat{d}_R(x) = (2\pi a)^{-1/2}\mathrm{e}^{\mathrm{i}[-\hat{\phi}(x)+\hat{\theta}(x)]}$ and $\hat{d}_L(x) = (2\pi a)^{-1/2}\mathrm{e}^{\mathrm{i}[\hat{\phi}(x)+\hat{\theta}(x)]}$ in terms of the bosonic fields satisfying the usual commutation relation $[\hat{\phi}(x),\, \partial_x\hat{\theta}(x')] = \mathrm{i}\pi\delta(x-x')$; the density operator $\hat{n}(x) = \hat{d}^\dagger(x)\hat{d}(x)$ is

$$\hat{n}(x) = -\frac{1}{\pi}\partial_x\phi(x) + \mathrm{e}^{-2\mathrm{i}k_F x}\hat{d}_R^\dagger(x)\hat{d}_L(x) + \mathrm{h.c.}; \tag{B.5}$$

moreover $\partial_x\hat{\phi}(x) = -\pi[\hat{d}_R^\dagger(x)\hat{d}_R(x) + \hat{d}_L^\dagger(x)\hat{d}_L(x)]$, $\partial_x\hat{\theta}(x) = \pi[\hat{d}_R^\dagger(x)\hat{d}_R(x) - \hat{d}_L^\dagger(x)\hat{d}_L(x)]$.

Within the bosonization formalism, the non-interacting Hamiltonian $\hat{H}_0$ becomes

$$\hat{H}_0 = \frac{v_F}{2\pi}\int \mathrm{d}x[(\partial_x\hat{\phi})^2 + (\partial_x\hat{\theta})^2] \tag{B.6}$$

where $v_F = \frac{a\Delta\epsilon}{2}\sin k_F a$. We recall here that $\nu = N/L = 1/2$ and $k_F = \pi/(2a)$; then $\mathrm{e}^{\pm 2\mathrm{i}k_F a} = -1$. The bosonization of the Hamiltonian term $\hat{H}_U^{(1)}$ is quite standard, see e.g. [69], and leads to

$$\hat{H}_U^{(1)} = 2\tilde{U}a\left[\frac{2}{\pi^2}(\partial_x\hat{\phi})^2 - \frac{2}{(2\pi a)^2}\cos 4\hat{\phi}(x)\right]. \tag{B.7}$$

The bosonization procedure of $\hat{H}_U^{(2)}$ is a bit more subtle. We preliminary consider the quantity $\hat{d}^\dagger(x+a)\hat{d}(x-a) + \mathrm{h.c.}$ that, up to a proper shift, can be rewritten as $\hat{d}^\dagger(x+2a)\hat{d}(x) + \mathrm{h.c.}$ Then we expand it in terms of the right and left operators taking into account that $\hat{d}_r(x+2a) \approx \hat{d}_r(x) + 2a\partial_x\hat{d}_r(x)$, with $r = R,\, L$. At the end of this procedure, we get four contributions $\hat{h}_{A,1}$, $\hat{h}_{A,2}$, $\hat{h}_{A,3}$, and $\hat{h}_B$ with

$$\hat{h}_{A,1} = -2\hat{d}_R^\dagger(x)\hat{d}_R(x) - 2\hat{d}_L^\dagger(x)\hat{d}_L(x) \tag{B.8}$$

$$\hat{h}_{A,2} = -2a\hat{d}_R^\dagger(x)\partial_x\hat{d}_R(x) - 2a\hat{d}_L^\dagger(x)\partial_x\hat{d}_L(x) \tag{B.9}$$

$$\hat{h}_{A,3} = -2a\partial_x\hat{d}_R^\dagger(x)\hat{d}_R(x) - 2a\partial_x\hat{d}_L^\dagger(x)\hat{d}_L(x) \tag{B.10}$$

$$\begin{aligned}\hat{h}_B = &-\mathrm{e}^{-2\mathrm{i}k_F x}[\hat{d}_R^\dagger(x)\hat{d}_L(x+2a) + \hat{d}_R^\dagger(x+2a)\hat{d}_L(x)] \\ &- \mathrm{e}^{2\mathrm{i}k_F x}[\hat{d}_L^\dagger(x)\hat{d}_R(x+2a) + \hat{d}_L^\dagger(x+2a)\hat{d}_R(x)].\end{aligned} \tag{B.11}$$

Now, recalling the identity (B.5), it is trivial to see that

$$\int \mathrm{d}x\; n(x+a)\hat{h}_{A,1} \approx \int \mathrm{d}x\left[-\frac{2}{\pi^2}(\partial_x\phi)^2\right] \tag{B.12}$$

with $\hat{\phi}(x+a) \approx \hat{\phi}(x) + a\partial_x\hat{\phi}$, we have approximated $\partial_x\hat{\phi}(x+a) \approx \partial_x[\hat{\phi}(x) + a\partial_x\hat{\phi}] \approx \partial_x\hat{\phi}$ and ignored terms of the form $\partial_x^2\hat{\phi}\partial_x\hat{\phi}$ and $\mathrm{e}^{\pm 2\mathrm{i}k_F x}$ fast oscillating terms Integrating by parts, we also observe that

$$\int \mathrm{d}x\; n(x+a)\hat{h}_{A,3} = -\int \mathrm{d}x\; (n(x+a)\hat{h}_{A,2} + \hat{C}) \tag{B.13}$$

with $\hat{C} \propto \partial_x\hat{\phi}\partial_x^2\hat{\phi}$. Then the first integral in equation (B.13) cancels with $\int \mathrm{d}x\; n(x+a)\hat{h}_{A,2}$, while the $\hat{C}$ term can be neglected.

Finally, we consider $\int \mathrm{d}x\; n(x+a)\hat{h}_B$. Neglecting fast oscillating terms $\mathrm{e}^{\pm 2\mathrm{i}k_F x}$, we get $\int \mathrm{d}x\; n(x+a)\hat{h}_B \approx \int \mathrm{d}x\; (\hat{h}_{\mathrm{non-osc}} + \hat{h}_{4k_F})$. The term $\hat{h}_{\mathrm{non-osc}}$ consists of the following non-oscillating terms:

$$\hat{d}_R^\dagger(x+a)\hat{d}_L(x+a)\hat{d}_L^\dagger(x)\hat{d}_R(x+2a) = \frac{1}{(2\pi a)^2}\mathrm{e}^{2\mathrm{i}a\partial_x\hat{\theta}} \tag{B.14}$$

$$\hat{d}_R^\dagger(x+a)\hat{d}_L(x+a)\hat{d}_L^\dagger(x+2a)\hat{d}_R(x) = \frac{1}{(2\pi a)^2}\mathrm{e}^{-2\mathrm{i}a\partial_x\hat{\theta}} \tag{B.15}$$

plus their hermitian conjugates; these terms can be rewritten as

$$\frac{1}{(2\pi a)^2}\mathrm{e}^{\pm 2\mathrm{i}a\partial_x\hat{\theta}} \approx \frac{1}{(2\pi a)^2}[1 \pm 2\mathrm{i}a\partial_x\hat{\theta} - 2a^2(\partial_x\hat{\theta})^2]. \tag{B.16}$$

The contribution $\hat{h}_{4k_F}$ consists of the following terms

$$\hat{d}_R^\dagger(x+a)\hat{d}_L(x+a)\hat{d}_R^\dagger(x)\hat{d}_L(x+2a) = \frac{1}{(2\pi a)^2}\mathrm{e}^{\mathrm{i}[4\hat{\phi}(x)+4a\partial_x\hat{\phi}+2a\partial_x\hat{\theta}]} \tag{B.17}$$

$$\hat{d}_R^\dagger(x+a)\hat{d}_L(x+a)\hat{d}_R^\dagger(x+2a)\hat{d}_L(x) = \frac{1}{(2\pi a)^2}e^{i[4\hat{\phi}(x)+4a\partial_x\hat{\phi}-2a\partial_x\hat{\theta}]} \tag{B.18}$$

and of their hermitian conjugates; when bosonized they give sine-Gordon terms of the form $\cos 4\hat{\phi}$. Collecting the results, we have

$$\hat{H}_U^{(2)} = -\tilde{U}a\left[-\frac{2}{\pi^2}(\partial_x\hat{\phi})^2 - \frac{2}{\pi^2}(\partial_x\hat{\theta})^2 + \frac{4}{(2\pi a)^2}\cos 4\hat{\phi}\right]. \tag{B.19}$$

Finally, the original Hamiltonian can be recast into the form

$$\hat{H} = \frac{u}{2\pi}\int dx\left[\frac{1}{K}(\partial_x\hat{\phi})^2 + K(\partial_x\hat{\theta})^2\right] - \frac{8\tilde{U}a}{(2\pi a)^2}\int dx\ \cos 4\hat{\phi} \tag{B.20}$$

provided we identify $u/K = v_F + 12\tilde{U}a/\pi$ and $uK = v_F + 4\tilde{U}a/\pi$.

Appendix C. Mean field approach

To calculate the critical interaction for which the system becomes gapped at filling $\nu = 1/2$ we proceed in the following way. We use a mean field approach to treat the correlated hopping term in the effective Hamiltonian of equation (26) and we define

$$\hat{H}_{corr} = -\frac{\tilde{U}}{2}\sum_j(\hat{n}_j\hat{d}_{j+1}^\dagger\hat{d}_{j-1} + \text{h.c.}). \tag{C.1}$$

Using the continuum limit operators $\hat{d}(x)$ and $\hat{d}^\dagger(x)$, we have:

$$\hat{H}_{corr} \propto \int dx\ \hat{n}(x+a)[\hat{d}^\dagger(x+2a)\hat{d}(x) + \text{h.c.}]. \tag{C.2}$$

Then, we define $\hat{n}(x) = n + \delta\hat{n}(x)$ and $\hat{d}^\dagger(x+2a)\hat{d}(x) = \chi + \delta\hat{\chi}(x)$, with $n(x) = \langle\hat{n}(x)\rangle$ and $\chi(x) = \langle\hat{d}^\dagger(x+2a)\hat{d}(x)\rangle$ such that

$$\hat{H}_{corr} \propto \int dx\ [n + \delta\hat{n}(x+a)][\chi + \delta\hat{\chi}(x) + \text{h.c.}]. \tag{C.3}$$

Neglecting quadratic fluctuation terms, trivial constants and an overall chemical potential, we obtain

$$\hat{H}_{corr} \propto n\int dx\ [\delta\hat{\chi}(x) + \text{h.c.}] \tag{C.4}$$

if we approximate $\hat{d}(x+2a) \approx \hat{d}(x) + 2a\partial_x\hat{d}(x)$, it is trivial to see that $\hat{H}_{corr} = 0$ (see also appendix B).

ORCID iDs

D Rossini https://orcid.org/0000-0002-9222-1913

References

[1] Altland A and Zirnbauer M R 1997 *Phys. Rev.* B **55** 1142
[2] Schnyder A P, Ryu S, Furusaki A and Ludwig A W W 2008 *Phys. Rev.* B **78** 195125
[3] Kitaev A 2009 *AIP Conf. Proc.* **1134** 22
[4] Hasan M Z and Kane C L 2010 *Rev. Mod. Phys.* **82** 3045
[5] Qi X-L and Zhang S-C 2011 *Rev. Mod. Phys.* **83** 1057
[6] Ludwig A W W 2016 *Phys. Scr.* **T168** 014001
[7] Wen X-G 2017 *Rev. Mod. Phys.* **89** 041004
[8] Cooper N R, Dalibard J and Spielman I B 2018 arXiv:1803.00249
[9] Struck J *et al* 2013 *Nat. Phys.* **9** 738
[10] Aidelsburger M, Lohse M, Schweizer C, Atala M, Barreiro J T, Nascimbéne S, Cooper N R, Bloch I and Goldman N 2015 *Nat. Phys.* **11** 162
[11] Kennedy C J, Burton W C, Chung W C and Ketterle W 2015 *Nat. Phys.* **11** 859
[12] Tai M E, Lukin A, Rispoli M, Schittko R, Menke T, Borgnia D, Preiss P M, Grusdt F, Kaufman A M and Greiner M 2017 *Nature* **546** 519
[13] Orignac E and Giamarchi T 2001 *Phys. Rev.* B **64** 144515
[14] Dhar A, Mishra T, Maji M, Pai R V, Mukerjee S and Paramekanti A 2013 *Phys. Rev.* B **87** 174501
[15] Tokuno A and Georges A 2014 *New J. Phys.* **16** 073005
[16] Greschner S, Piraud M, Heidrich-Meisner F, McCulloch I P, Schollwöck U and Vekua T 2016 *Phys. Rev.* A **94** 063628
[17] Kolley F, Piraud M, McCulloch I, Schollwöck U and Heidrich-Meisner F 2015 *New J. Phys.* **17** 092001
[18] Piraud M, Heidrich-Meisner F, McCulloch I P, Greschner S, Vekua T and Schollwöck U 2015 *Phys. Rev.* B **91** 140406(R)
[19] Barbarino S, Taddia L, Rossini D, Mazza L and Fazio R 2015 *Nat. Commun.* **6** 8134
[20] Barbarino S, Taddia L, Rossini D, Mazza L and Fazio R 2016 *New J. Phys.* **18** 035010
[21] Taddia L, Cornfeld E, Rossini D, Mazza L, Sela E and Fazio R 2017 *Phys. Rev. Lett.* **118** 230402

[22] Orignac E, Citro R, Di Dio M and De Palo S 2017 *Phys. Rev.* B **96** 014518
[23] Citro R, De Palo S, Di Dio M and Orignac E 2018 *Phys. Rev.* B **97** 174523
[24] Atala M, Aidelsburger M, Lohse M, Barreiro J T, Paredes B and Bloch I 2014 *Nat. Phys.* **10** 588
[25] Mancini M *et al* 2015 *Science* **349** 1510
[26] Stuhl B K, Lu H-I, Aycock L M, Genkina D and Spielman I B 2015 *Science* **349** 1514
[27] Jaksch D and Zoller P 2003 *New. J. Phys.* **5** 56
[28] Cazalilla M A and Rey A M 2014 *Rep. Prog. Phys.* **77** 124401
[29] Livi L F *et al* 2016 *Phys. Rev. Lett.* **117** 220401
[30] Kolkowitz S, Bromley S L, Bothwell T, Wall M L, Marti G E, Koller A P, Zhang X, Rey A M and Ye J 2017 *Nature* **542** 66
[31] Han J H, Kang J H and Shin Y 2019 *Phys. Rev. Lett.* **122** 065303
[32] Kang J H, Han J H and Shin Y 2018 *Phys. Rev. Lett.* **121** 150403
[33] Wall M L, Koller A P, Li S, Zhang X, Cooper N R, Ye J and Rey A M 2016 *Phys. Rev. Lett.* **116** 035301
[34] Barbarino S, Dalmonte M, Fazio R and Santoro G E 2018 *Phys. Rev.* A **97** 013634
[35] Hughes T L, Prodan E and Bernevig B A 2011 *Phys. Rev.* B **83** 245132
[36] Chiu C-K, Yao H and Ryu S 2013 *Phys. Rev.* B **88** 075142
[37] Chiu C-K, Teo J C Y, Schnyder A P and Ryu S 2016 *Rev. Mod. Phys.* **88** 035005
[38] Hubbard J 1978 *Phys. Rev.* B **17** 494
[39] Pokrovsky V L and Uimin G V 1978 *J. Phys.* C **11** 3535
[40] Wilczek F and Zee A 1984 *Phys Rev. Lett.* **52** 2111
[41] Chruscinski D and Jamiolkowski A 2004 *Geometric Phases in Classical and Quantum Mechanics* (Berlin: Springer)
[42] Niu Q, Thouless D J and Wu Y-S 1985 *Phys. Rev.* B **31** 3372
[43] Resta R 1994 *Rev. Mod. Phys.* **66** 899
[44] Fidkowski L 2010 *Phys. Rev. Lett.* **104** 130502
[45] Pollmann F, Turner A M, Berg E and Oshikawa M 2010 *Phys. Rev.* B **81** 064439
[46] Turner A M, Pollmann F and Berg E 2011 *Phys. Rev.* B **83** 075102
[47] Guo H, Shen S-Q and Feng S 2012 *Phys. Rev.* B **86** 085124
[48] Budich J C and Ardonne E 2013 *Phys. Rev.* B **88** 035139
[49] Su W-P, Schrieffer J R and Heeger A J 1979 *Phys. Rev. Lett.* **42** 1698
[50] Creutz M 1999 *Phys. Rev. Lett.* **83** 2636
[51] Guo H and Shen S-Q 2011 *Phys. Rev.* B **84** 195107
[52] Jünemann J, Piga A, Ran S-J, Lewenstein M, Rizzi M and Bermudez A 2017 *Phys. Rev.* X **7** 031057
[53] Essler F H L, Frahm H, Göhmann F, Klümper A and Korepin V E 2005 *The One-Dimensional Hubbard Model* (Cambridge: Cambridge University Press)
[54] Velasco G C and Paredes B 2017 *Phys. Rev. Lett.* **119** 115301
[55] Carr S T, Narozhny B N and Nersesyan A A 2006 *Phys. Rev.* B **73** 195114
[56] Stoudenmire E M, Alicea J, Starykh O A and Fisher M P A 2011 *Phys. Rev.* B **84** 014503
[57] Huang C-W, Carr S T, Gutman D, Shimshoni E and Mirlin A D 2013 *Phys. Rev.* B **88** 125134
[58] Kraus C V, Dalmonte M, Baranov M A, Laeuchli A M and Zoller P 2013 *Phys. Rev. Lett.* **111** 173004
[59] Petrescu A, Piraud M, Roux G, McCulloch I P and Le Hur K 2017 *Phys. Rev.* B **96** 014524
[60] Tovmasyan M, Peotta S, Törmä P and Huber S D 2016 *Phys. Rev.* B **94** 245149
[61] Calvanese Strinati M, Cornfeld E, Rossini D, Barbarino S, Dalmonte M, Fazio R, Sela E and Mazza L 2017 *Phys. Rev.* X **7** 021033
[62] Santos R A and Béri B 2018 arXiv:1806.02874
[63] Rachel S 2018 *Rep. Prog. Phys.* **81** 116501
[64] Boada O, Celi A, Latorre J I and Lewenstein M 2012 *Phys. Rev. Lett.* **108** 133001
[65] Celi A, Massignan P, Ruseckas J, Goldman N, Spielman I B, Juzeliūnas G and Lewenstein M 2014 *Phys. Rev. Lett.* **112** 043001
[66] Lanczos C 1950 *J. Res. Natl. Bur. Stand.* **45** 255
[67] White S R 1992 *Phys. Rev. Lett.* **69** 2863
[68] Schollwöck U 2005 *Rev. Mod. Phys.* **77** 259
[69] Giamarchi T 2004 *Quantum Physics in One Dimension* (Oxford: Oxford Science Publications)
[70] Dalmonte M, Pupillo G and Zoller P 2010 *Phys. Rev. Lett.* **105** 140401
[71] Takahashi M 2005 *Thermodynamics of One-Dimensional Solvable Models* (Cambridge: Cambridge University Press)
[72] Stoudenmire E M, Alicea J, Starykh O A and Fisher M P A 2011 *Phys. Rev.* B **84** 014503
[73] Kraus C V, Dalmonte M, Baranov M A, Läuchli A M and Zoller P 2013 *Phys. Rev. Lett.* **111** 173004
[74] Kawamoto N and Smit J 1981 *Nuc. Phys.* **192** 100
[75] Privman V 1990 *Finite Size Scaling and Numerical Simulations of Statistical Systems* (Singapore: World Scientific)